

This work is on a Creative Commons Attribution-NonCommercial-NoDerivatives 4.0 International (CC BY-NC-ND 4.0) license, <https://creativecommons.org/licenses/by-nc-nd/4.0/>. Access to this work was provided by the University of Maryland, Baltimore County (UMBC) ScholarWorks@UMBC digital repository on the Maryland Shared Open Access (MD-SOAR) platform.

Please provide feedback

Please support the ScholarWorks@UMBC repository by emailing scholarworks-group@umbc.edu and telling us what having access to this work means to you and why it's important to you. Thank you.

Independent vector analysis for subspace analysis of multi-subject medical imaging data

Qunfang Long*, Suchita Bhinge, Vince D. Calhoun, and Tülay Adalı

Abstract—The extraction of common and distinct biomedical signatures among different populations allows for a more detailed study of the group-specific as well as distinct information of different populations. A number of subspace analysis algorithms have been developed and successfully applied to data fusion, however they are limited to joint analysis of only a couple of datasets. Since subspace analysis is very promising for analysis of multi-subject medical imaging data as well, we focus on this problem and propose a new method based on independent vector analysis (IVA) for common subspace extraction (IVA-CS) for multi-subject data analysis. IVA-CS leverages the strength of IVA in identification of a complete subspace structure across multiple datasets along with an efficient solution that uses only second-order statistics. We propose a subset analysis approach within IVA-CS to mitigate issues in estimation in IVA due to high dimensionality, both in terms of components estimated and the number of datasets. We introduce a scheme to determine a desirable size for the subset that is high enough to exploit the dependence across datasets and is not affected by the high dimensionality issue. We demonstrate the success of IVA-CS in extracting complex subset structures and apply the method to analysis of functional magnetic resonance imaging data from 179 subjects and show that it successfully identifies shared and complementary brain patterns from patients with schizophrenia (SZ) and healthy controls group. Two components with linked resting-state networks are identified to be unique to the SZ group providing evidence of functional dysconnectivity. IVA-CS also identifies subgroups of SZs that show significant differences in terms of their brain networks and clinical symptoms.

Index Terms—Independent vector analysis, subspace analysis, multi-subject medical imaging data, functional magnetic resonance imaging, heterogeneity of schizophrenia

I. INTRODUCTION

The study of neuroimaging data from patients and healthy controls is prevalent in the neuroimaging field with a goal to identify differences in the brain function of these two groups ([1]–[3]) and data-driven techniques based on matrix decompositions are being increasingly used for the task ([4], [5]). Identification of common and distinct subspaces from multiple datasets transforms the high dimensional datasets into

lower dimensional joint and disjoint subspaces, and allows for a more detailed analysis of the group-specific as well as distinct information. In these models, the assumption is that each observed dataset is explained by a sum of linearly mixed latent variable models. The common subspace is defined as a subset of latent variables that are highly correlated across the given datasets. The distinct subspace is a subset of latent variables that have very low correlation to each other. The joint subspaces bring the datasets to a common ground, thus allowing for a fair and reliable comparison among different population groups. Meanwhile the distinct components can be used to study individual differences such as the unique connection pattern of a patient with mental disease.

Along with identifying a common subspace comprised of components correlated across all subjects, the extraction of common components across a subgroup of subjects is also of interest. Clinical heterogeneity of patients with mental disorders, especially in schizophrenia has been recognized ([6]–[8]), and there has been significant interest in studying their subtypes ([9]–[11]). The study of subtypes can be made possible by identifying subgroups of patients that share specific common information and can help better understand the uncertainty in the need of precision medicine ([12]) during clinical diagnosis and treatment. Subtypes of schizophrenia have been well studied using genetic information ([9], [11]) but not yet using other neuroimaging modalities such as functional magnetic resonance imaging (fMRI) data, which has been successfully used in the study of schizophrenia ([10], [13], [14]). The common subspace analysis motivates us to find a way to identify subgroups of patients with subtypes of schizophrenia by summarizing their shared information.

Given the importance of common and distinct subspace analysis in medical image analysis, a number of recent studies had a focus on this aspect, in particular for fusion of different modalities such as fMRI, structural MRI and electroencephalograph, or of fMRI data from different tasks ([15]–[22]). However these cases have only been demonstrated for joint decomposition of a small number of datasets. As we have discussed, distinct and common subspace analysis also promises to be attractive for multi-subject analyses. The models used for identification of common and distinct subspaces in fusion study have not been well-studied in the context of the joint analysis of more than a couple of datasets. Multi-subject data analysis involves joint analysis of at least tens, or more typically hundreds of subjects. A recently proposed method Shared and Subject-Specific Dictionary Learning (ShSSDL) ([23]) targets multi-subject task fMRI analysis and identifies shared components across subjects as well as subject-specific com-

Qunfang Long, Suchita Bhinge, and Tülay Adalı are with the Department of Computer Science and Electrical Engineering, University of Maryland Baltimore County, Baltimore, MD 21250, USA. E-mail: {qunfangl, adali}@umbc.edu (see <http://mlsp.umbc.edu/>).

Vince D. Calhoun is with the Mind Research Network and the Department of Electrical and Computer Engineering, University of New Mexico, Albuquerque, NM 87131, and the Tri-institutional Center for Translational Research in Neuroimaging and Data Science (TReNDS), Georgia State University, Georgia Institute of Technology, Emory University, Atlanta, GA.

To appear in NeuroImage: Q. Long, S. Bhinge, V. D. Calhoun, and T. Adalı. (2020) “Independent Vector Analysis for Common Subspace Analysis: Application to Multi-subject fMRI Data Yields Meaningful Subgroups of Schizophrenia.” *NeuroImage*.

ponents. However, ShSSDL assumes common time courses across datasets and is not able to identify components that are common across subgroups of subjects. Another ICA-based algorithm, hierarchical ICA ([24]), simultaneously estimates the population-level and subject-specific sources. However, the complexity of the density model used in hierarchical ICA grows when the number of datasets increases and it does not account for the dependence structure of these sources.

In this work, we propose a new method, which we call, independent vector analysis (IVA) for common subspace extraction (IVA-CS) to extract subspaces from large-scale datasets and demonstrate its successful application to the analysis of fMRI data collected from 179 subjects. IVA ([25], [26]) has been successfully used for multi-subject medical imaging data analysis such as fMRI data ([27]–[29]) and has been shown to effectively capture subject variability compared to the group independent component analysis (ICA) approach ([30], [31]). IVA extends ICA to multiple datasets and makes effective use of the dependence across the datasets through the definition of a source component vector (SCV), making it an attractive choice for subspace analysis. Through the selection of an effective density model for the SCV, with IVA, one can model and estimate the statistical dependence across datasets. Additionally, the strong identification condition of IVA—*i.e.*, the ability to uniquely identify the underlying latent variables—enables the preservation of subspace structure even using only second-order statistics (SOS) as we demonstrate by simulation results in Section IV. IVA with multivariate Gaussian distribution (IVA-G) ([32]) is an IVA algorithm that takes only SOS into consideration by assuming a multivariate Gaussian distribution for each SCV and provides efficient estimation with reliable convergence due to its desirable analytical properties. We show that IVA-CS using IVA-G (IVA-G-CS) is powerful in discovering the subspace structure and estimating the subspaces through a careful study of the correlation structure of SCVs.

Furthermore, IVA-CS helps mitigate the high dimensionality issue of IVA and enables a reliable estimation of the latent sources from multi-subject data. The curse of dimensionality of IVA notes that the performance of IVA degrades with increase in the number of sources, *i.e.*, the IVA model order, and datasets for a fixed number of samples ([33]). Hence for a high model order and relatively large number of datasets, IVA requires a proportionally large number of data samples for efficient estimation of the demixing matrices. However, the number of samples is fixed in many real-world applications such as fMRI data analysis since the resolution of the data is predetermined. On the other hand, the dependent information across datasets is not sufficient for IVA to exploit in the case with a relatively small number of datasets. Thus, in order to reliably estimate the sources with a given number of samples, we need to determine the desirable number of datasets that is high enough to exploit the dependence across datasets and is not affected by issues regarding high dimensionality. For the purpose of finding the optimal number of datasets to be used in a single IVA decomposition, we estimate and fix the model order for the data, and explore for the number of datasets, *i.e.*, number of subjects. We then divide the entire data into

subsets of subjects and perform IVA on each subset to identify common subspace. This defines the first stage of IVA-CS, subset analysis. The common components from each subset are further compared to find the consistent common components for all subjects as well as subgroups of subjects in a group, which then defines the second stage of IVA-CS, *i.e.*, common subspace identification.

We study the ability of IVA to preserve the subspace structure using simulated data and demonstrate that IVA identification condition enables successful recovery of the structure of all subspaces using only SOS. We compare the results to the commonly used multiset canonical correlation analysis (MCCA) ([34]) for joint data analysis that also uses SOS ([35], [36]). Then, we apply IVA-CS to real fMRI data collected from 88 patients with schizophrenia (SZ) and 91 healthy controls (HC) and show that IVA-CS extracts interpretable common components for the SZ and HC groups separately. These common components are typical resting-state network (RSN) components such as sensorimotor, frontoparietal and default mode network, which are also found in previous studies ([37], [38]). The results show that two components unique to the SZ group include two different interesting RSNS. The first one merges the motor cortex (precentral and postcentral gyrus) and the auditory cortex (superior temporal gyrus) and the other one merges the precuneus gyrus and the right frontoparietal network. Analysis of the correlation matrices of group-specific components helps us identify a number of subgroups of patients that show significant difference in terms of spatial activation of different brain networks such as cingulate gyrus, secondary visual gyrus, primary somatosensory and motor cortex, and inferior frontal gyrus. This provides neurobiological support for the heterogeneity of schizophrenia. The subgroups also demonstrate significant differences in clinical symptoms that are measured by the positive and negative syndrome scale (PANSS) scores ([39]) and possess unique dominant and absent symptoms. PANSS scores are analyzed synthetically, rather than individually since the self-reported symptom scores are, in general, subjective and noisy, and hence not effective in terms of categorization of disease. These findings emphasize the importance of interpreting subtypes of schizophrenia in terms of both the neuroimaging data analysis and the clinically diagnostic data.

The rest of the paper is organized as follows. Section II presents the background of IVA. Section III introduces the details of the subset analysis and common subspace identification of the proposed IVA-CS method. Section IV-A and Section IV-B show the simulated results and the application to real fMRI data analysis separately. Section VI summarizes the work and points out future directions.

II. BACKGROUND

A. Independent Vector Analysis

In most real-world applications the observed data consists of multiple datasets such as the fMRI data that is collected from multiple subjects. Enabling an analysis of multiset data to leverage its rich information especially across the datasets is important. ICA is a data-driven blind source separation

technique that is designed for a single dataset with the assumption that the observed data is a linear mixture of latent (statistically) independent sources ([40]). It has proven powerful in recovering the independent brain networks from fMRI data ([41]–[43]). IVA extends ICA to the joint analysis of multiple datasets by additionally taking into account the dependence across datasets ([25], [26], [41]).

Suppose there are K datasets collected from K subjects each containing V samples. IVA assumes that each dataset is a linear mixture of N independent sources,

$$\mathbf{x}^{[k]}(v) = \mathbf{A}^{[k]} \mathbf{s}^{[k]}(v), \quad 1 \leq k \leq K, \quad 1 \leq v \leq V, \quad (1)$$

where $\mathbf{X}^{[k]} = [\mathbf{x}^{[k]}(1), \mathbf{x}^{[k]}(2), \dots, \mathbf{x}^{[k]}(V)] \in \mathbb{R}^{N \times V}$, $\mathbf{S}^{[k]} = [\mathbf{s}^{[k]}(1), \mathbf{s}^{[k]}(2), \dots, \mathbf{s}^{[k]}(V)] \in \mathbb{R}^{N \times V}$ and $\mathbf{A}^{[k]} \in \mathbb{R}^{N \times N}$ denote the observed dataset, the set of independent sources, and the invertible mixing matrix respectively. A general model of IVA is shown in Figure 1. In addition to the assumption of independence among sources within a dataset, IVA makes effective use of dependence across multiple datasets by defining an SCV as $\mathbf{s}_n(v) = [s_n^{[1]}(v), s_n^{[2]}(v), \dots, s_n^{[K]}(v)]^T \in \mathbb{R}^{K \times 1}$, $1 \leq n \leq N$, by collecting corresponding components, where $\mathbf{s}_n^{[k]} \in \mathbb{R}^{V \times 1}$ is the n th source from the k th dataset. ICA can be achieved by minimizing the mutual information among the individual latent sources. After extending to multiple datasets, an IVA solution finds K demixing matrices by minimizing the mutual information among the SCVs, which results in the following cost function

$$\begin{aligned} \mathcal{C}_{\text{IVA}}(\mathbf{W}) &= \sum_{n=1}^N \mathcal{H}(\mathbf{y}_n) - \sum_{k=1}^K \log|\det \mathbf{W}^{[k]}| \\ &= - \sum_{n=1}^N \mathbb{E}\{\log p_n(\mathbf{y}_n)\} - \sum_{k=1}^K \log|\det \mathbf{W}^{[k]}| \end{aligned} \quad (2)$$

such that the estimated sources of each dataset are obtained as $\mathbf{y}^{[k]}(v) = \mathbf{W}^{[k]} \mathbf{x}^{[k]}(v)$ for $k = 1, \dots, K$, where $\mathbf{W} = \{\mathbf{W}^{[1]}, \mathbf{W}^{[2]}, \dots, \mathbf{W}^{[K]}\}$ denotes the demixing matrices, \mathbf{y}_n denotes the estimated SCV, and $\mathcal{H}(\cdot)$ denotes the (differential) entropy. Minimization of (2) is equivalent to maximization of likelihood through the general asymptotic equipartition property ([41])

$$\mathcal{L}_{\text{IVA}}(\mathbf{W}) = \sum_{n=1}^N \log(p_n(\mathbf{Y}_n)) + V \sum_{k=1}^K \log|\det \mathbf{W}^{[k]}|, \quad (3)$$

where $\mathbf{Y}_n = [\mathbf{y}_n(1), \mathbf{y}_n(2), \dots, \mathbf{y}_n(V)]$, and $p_n(\cdot)$ denotes the multivariate probability distribution of n th SCV. In both (2) and (3) the term that is constant with respect to \mathbf{W} associated with the observed data \mathbf{X} is ignored. For simplicity, in the rest of the paper we consider the simpler independent and identical distribution case and do not take sample dependence into account.

B. Identification Condition for IVA

Identification condition of IVA is studied by analyzing the Fisher information matrix of the objective function (3) with respect to the demixing matrices \mathbf{W} ([41], [44]). Compared

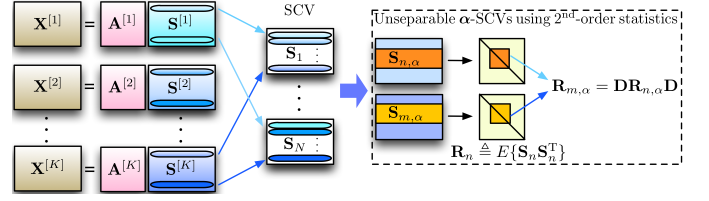


Fig. 1: IVA model and an example of two unseparable α -SCVs

with the identification condition of ICA that is associated with two individual sources, the identification condition of IVA is introduced for two SCVs. It is shown that the identification condition of IVA depends on the second-order statistics (SOS) of subsets of sources in an SCV. If the SOS defined through covariance matrices provide the required diversity across SCVs, the SCVs are separable even when they are multivariate Gaussian distributed since their SOS can be accurately captured by any type of multivariate distribution prior. We define an α -SCV as an SCV with a particular subset of source components that are K_α -dimensional multivariate distributed and independent from the complementing subset in the same SCV. Note that all sources are assumed to have unit variance and zero mean for simplicity. Let $\alpha \in \mathbb{N}^{K_\alpha}$ be a subset of source indices within an SCV, where $0 \leq K_\alpha \leq K$. The complementing subset of α in $1, 2, \dots, K$ is denoted as $\alpha^c \in \mathbb{N}^{K-K_\alpha}$. In two arbitrary α -SCVs, the subsets of sources, $\mathbf{S}_{n, \alpha} \in \mathbb{R}^{K_\alpha \times V}$ and $\mathbf{S}_{m, \alpha} \in \mathbb{R}^{K_\alpha \times V}$, cannot be identified if and only if there exists a full rank diagonal matrix $\mathbf{D} \in \mathbb{R}^{K_\alpha \times K_\alpha}$ such that

$$\mathbf{R}_{m, \alpha} = \mathbf{D} \mathbf{R}_{n, \alpha} \mathbf{D}, \quad (4)$$

where $\mathbf{R}_{n, \alpha} \triangleq \mathbb{E}\{\mathbf{S}_{n, \alpha} \mathbf{S}_{n, \alpha}^T\} \in \mathbb{R}^{K_\alpha \times K_\alpha}$ refers to the correlation matrix of the subset of sources ([44]). This suggests that the correlation matrices of the subsets of sources in two unseparable α -SCVs have the same structure but different scaling. If an IVA algorithm only takes SOS into consideration, any subset of sources within an SCV that possess this property will not be separated into individual ones. An example of two unseparable α -SCVs is shown in Figure 1. The change in value of K_α indicates that two SCVs can be unseparable either in whole or in subsets of components. However, this is no longer a problem when other types of diversity, such as higher than second-order statistics (HOS) and sample dependence, of the data are taken into consideration.

The most commonly used blind source separation algorithm for multiple datasets is multiset canonical correlation analysis (MCCA) ([34], [35]) which is based on SOS only. Five cost functions, *i.e.*, GENVAR, MINVAR, MAXVAR, SUMVAR, and SSQCOR, are introduced in ([34]) for maximizing correlation among linearly transformed multiple datasets, which in IVA formulation are the SCVs. MCCA adopts a deflationary approach to estimate one SCV at each time hence its cost function is associated with the correlation matrix of a single SCV. Since the correlation among the sources within each SCV is maximized, the goal for each cost—mostly ad-hoc in nature—is trying to make the correlation matrix as ill-conditioned as possible. MCCA with GENVAR cost function (MCCA-GENVAR) can be shown to have the same cost function as IVA-G ([32]) if the demixing matrices are assumed

to be orthogonal ([41]). Both MCCA and IVA-G make use of only the SOS of the data. The identification condition for MCCA is given by pairwise correlation values

$$\forall k, l \in \{1, 2, \dots, K\}, |r_{k,l}^{[m]}| \neq |r_{k,l}^{[n]}|, 1 \leq m < n \leq N, \quad (5)$$

where $r_{k,l}^{[n]}$ is the element of \mathbf{R}_n ([35]). Hence MCCA cannot preserve the structure of SCVs. In contrast, IVA-G has a more general identification condition given in (4) that is synchronized for all SCVs, which enables one to discover subspace structures as we demonstrate by simulation results in Section IV-A.

C. IVA Algorithms

To maximize the likelihood, besides \mathbf{W} , we need to estimate the multivariate density function of SCV. The selection of the multivariate distribution, $p_n(\mathbf{y}_n)$, determines whether SOS and/or HOS of the data are taken into consideration. IVA-G assumes that the sources in an SCV are multivariate Gaussian distributed and only takes SOS into consideration ([32]). This assumption guarantees a positive definite Hessian matrix of the cost at the global optimum hence providing a reliable estimation by using second-order optimization techniques such as using Newton updates. IVA with multivariate Laplacian distribution (IVA-L) assumes each SCV is modeled by the multivariate Laplacian distribution ([25], [26]). The assumption is that the correlation matrix of an SCV is identity thus taking only HOS into consideration. IVA with multivariate generalized Gaussian distribution (IVA-MGGD) on the other hand assumes that an SCV is multivariate generalized Gaussian distributed ([44]–[46]). IVA-MGGD calculates the whole correlation matrix and estimates the shape parameter of the MGGD that models each SCV, making it possible to take both SOS and HOS into consideration. As a consequence, this algorithm is computationally complex but provides good performance. IVA-L with SOS (IVA-L-SOS) ([33]) calculates the whole correlation matrix of each SCV as in IVA-MGGD but fixes the shape parameter to 0.5 to model a multivariate Laplacian distribution which is a good match for fMRI sources. Hence it takes both SOS and HOS into consideration and simplifies the computational complexity compared with IVA-MGGD. Both IVA-G and IVA-L-SOS have proven powerful in extracting interpretable source components when applied to medical imaging data analysis ([16], [32], [33]).

III. IVA FOR SUBSPACE ANALYSIS

Common and distinct subspace analysis has proven useful in identifying distinct biomedical signatures of different populations in order to better understand the unique features of different brain disorders. Most subspace analysis algorithms introduced to date that have shown superior performance are designed specially for fusion study where only a few datasets are analyzed ([15]–[20]). However, these models become extraordinarily complex as the data size increases to tens or even hundreds of datasets. Most medical imaging data like fMRI data is collected from tens or hundreds of subjects and a joint analysis of the multiset data enables one to leverage its rich information especially across the datasets. This motivates

the exploration of an algorithm which can identify common and distinct subspaces from relatively large-scale datasets.

We assume that the source space of the observed data consists of three sets of SCVs. The first set of SCVs, $\{\mathbf{Y}_{Cn} = [\mathbf{y}_{Cn}^{[1]}, \dots, \mathbf{y}_{Cn}^{[K]}]^T\}, 1 \leq n \leq N_C$, define the common subspace where the sources within each SCV are highly correlated (across all datasets) and the third set of SCVs, $\{\mathbf{Y}_{Dn} = [\mathbf{y}_{Dn}^{[1]}, \dots, \mathbf{y}_{Dn}^{[K]}]^T\}, 1 \leq n \leq N_D$, consist of low correlated sources (correlation values less than σ_r^2) as shown in Figure 2(a). Another set of group-specific SCVs, $\{\mathbf{Y}_{Gn} = [\mathbf{y}_{Gn}^{[1]}, \dots, \mathbf{y}_{Gn}^{[K]}]^T\}, 1 \leq n \leq N_G$, can be used to determine subgroups of subjects that have more highly correlated RSNs in an unsupervised manner. Therefore, the observed dataset for the k th subject is a mixture of three types of sources:

$$\begin{aligned} \mathbf{X}^{[k]} &= \hat{\mathbf{A}}^{[k]} \mathbf{Y}^{[k]} \\ &= \hat{\mathbf{A}}_C^{[k]} \mathbf{Y}_C^{[k]} + \hat{\mathbf{A}}_G^{[k]} \mathbf{Y}_G^{[k]} + \hat{\mathbf{A}}_D^{[k]} \mathbf{Y}_D^{[k]} \\ &= [\hat{\mathbf{A}}_C^{[k]} \quad \hat{\mathbf{A}}_G^{[k]} \quad \hat{\mathbf{A}}_D^{[k]}] \begin{bmatrix} \mathbf{Y}_C^{[k]} \\ \mathbf{Y}_G^{[k]} \\ \mathbf{Y}_D^{[k]} \end{bmatrix}, \quad k = 1, 2, \dots, K, \end{aligned} \quad (6)$$

where $\hat{\mathbf{A}}_C^{[k]}$, $\hat{\mathbf{A}}_G^{[k]}$, and $\hat{\mathbf{A}}_D^{[k]}$ are corresponding estimated mixing matrices of the common sources $\mathbf{Y}_C^{[k]} = [\mathbf{y}_{C1}^{[k]}, \dots, \mathbf{y}_{CN_C}^{[k]}]^T$, the sources $\mathbf{Y}_G^{[k]} = [\mathbf{y}_{G1}^{[k]}, \dots, \mathbf{y}_{GN_G}^{[k]}]^T$ that compose the group-specific SCVs, and the distinct sources $\mathbf{Y}_D^{[k]} = [\mathbf{y}_{D1}^{[k]}, \dots, \mathbf{y}_{DN_D}^{[k]}]^T$, respectively.

In this work, we propose a new method called IVA-CS that is able to extract subspaces from at least couple of hundreds of datasets. IVA-CS leverages the strength of IVA that its identification condition enables successful preservation of the SCV structure, which makes it highly effective for subspace analysis. However, IVA suffers from the curse of dimensionality when applied to real-world applications with a high number, *e.g.*, hundreds, of datasets such as in multi-subject fMRI data analysis. In this scenario since the number of samples (voxels) is fixed, as the number of datasets and the number of sources increases, it does not guarantee an accurate estimation of the demixing matrices \mathbf{W} and calculation of SCV correlation matrices any more. Therefore, our IVA-CS method is composed of two stages, (i) subset analysis and (ii) common subspace identification. The subset analysis stage overcomes the challenge of dimensionality issue by first performing multiple individual IVA decompositions on subsets of subjects that are randomly sampled from the population. The exploration of subset size, K , will be introduced in detail in Section IV-B2. The common subspace identification stage determines a consistent common subspace for the whole population as well as a set of the group-specific SCVs. The details of IVA-CS method are given next.

A. IVA-CS: Subset Analysis

The flowchart of IVA-CS is shown in Figure 2(b). In subset analysis, R subsets of K subjects are randomly selected from all subjects of a group. IVA is performed on each subset yielding N SCVs. We define the whole signal space as \mathcal{Y}

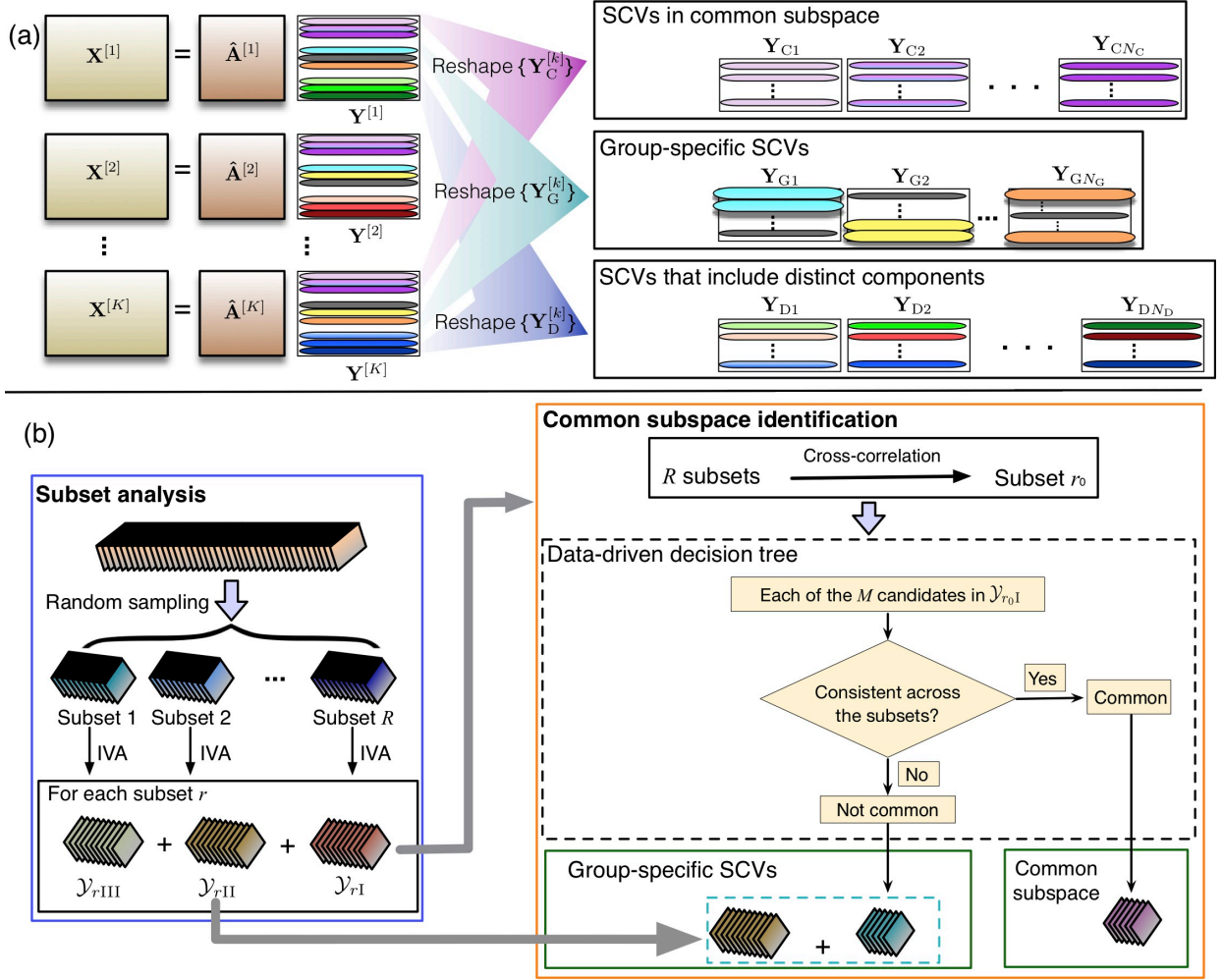


Fig. 2: The definition of common subspace and other two sets of SCVs in signal space (a) and the subset analysis and common subspace identification of IVA-CS (b). The number of SCVs in each of the three sets in (a) are denoted by N_C , N_G and N_D separately.

that includes all N estimated sources, where $\mathbf{y}_n^{[k]}$ denotes the n th source of the k th dataset. For each subset, its signal space is denoted as $\mathcal{Y}_r, 1 \leq r \leq R$. Note that all source components are normalized to have unit variance and zero mean hence their covariance values and correlation values coincide. For each SCV we compute a $K \times K$ correlation matrix with $K \times (K - 1)/2$ distinct correlation values. Using these correlation values, we can study how close these components are to each other and determine whether the corresponding source component is common across all the datasets or not. For an SCV corresponding to the common component, we expect that all the correlation values are significantly high. We measure the “commonality” of an SCV by computing the ratio of the number of correlation values that are greater than σ_t^2 , an empirically determined threshold, to the total number of correlation values for each SCV as follows,

$$q = \frac{N_{\sigma_t^2}}{K(K - 1)/2}, \quad (7)$$

where $N_{\sigma_t^2}$ denotes the number of correlation values that are greater than σ_t^2 in the correlation matrix of an SCV. An SCV corresponding to a common component is expected to have high commonality hence the value of q is close to 1. Another

relevant metric is “dissimilarity” which is defined as the ratio of the number of low correlation values to the number of high correlation values

$$\tilde{q} = \frac{K(K - 1)/2 - N_{\sigma_t^2}}{N_{\sigma_t^2}}. \quad (8)$$

The dissimilarity, the value of \tilde{q} , for a common SCV is expected to be close to 0.

For each subset $r, r = 1, \dots, R$, N SCVs are sorted in descending order by the mean value of the correlation, which roughly arranges the SCVs from those with high source correlation to those with low source correlation. The number of common SCVs in each subset, M_r , is determined as the largest number that allows for most of the first M_r SCVs having $q \geq \delta_1$ and $\tilde{q} \leq \delta_2$. Here not all the M_r SCVs are required to satisfy the criteria, seeking to allow flexibility for a further examination of the commonness of these components. After determining the first subspace $\mathcal{Y}_{r\text{I}}$ that is spanned by the M_r common SCVs for each subset, P percent of the remaining SCVs that have a mix of both high and low correlation values forms the second subspace $\mathcal{Y}_{r\text{II}}$. The other SCVs form the

third subspace $\mathcal{Y}_{r\text{III}}$, which is the distinct subspace.

B. IVA-CS: Common Subspace Identification

The second stage, common subspace identification has the goal to find a consistent common subspace \mathcal{Y}_C for all subjects of a group. To enable a comprehensive comparison across R subsets, we adjust the number of components in the subspace $\mathcal{Y}_{r\text{I}}$ to be common as M across all subsets. The M SCVs are candidates for the common subspace identification. The value of M is determined as the largest value of M_r , seeking to select as many candidates as possible. The mean component, $\mathbf{y}_{mr}, m = 1, \dots, M, r = 1, \dots, R$, is calculated by averaging the K components in the m th SCV for each subset r . The cross-correlation of each mean component is defined as the average correlation with its corresponding components in the other $R - 1$ subsets:

$$\rho_{mr} = \frac{1}{R-1} \sum_{l \neq r} |\rho_{mrl}|, \quad (9)$$

where $\rho_{mrl}, 1 \leq l \leq R, l \neq r$ is the Pearson correlation coefficient between the mean components \mathbf{y}_{mr} and \mathbf{y}_{ml} . For each subset, its cross-correlation is defined as the average cross-correlation of its M mean components

$$\rho_r = \frac{1}{M} \sum_m \rho_{mr}. \quad (10)$$

The subset r_0 with the most consistent components is selected as the one with the largest cross-correlation ρ_r and is used to identify the common subspace for all the subjects. The identified common components should be not only common across the subjects within subset r_0 but also consistent across all subsets. To achieve this goal, we use a data-driven decision tree to determine whether a component is common or not as shown in Figure 2(b). A threshold t is determined from the $M(R-1)$ cross-correlation values. For each candidate, if more than a given percentage of its cross-correlation values are higher than t , it is determined to be a common component. First, the determined common component comes from the first subspace of subset r_0 which means it is common across all the subjects within subset r_0 . Second, this decision tree ensures that this component is correlated with its corresponding components from most of all the subsets hence it is consistent across subsets. The identified common subspace of all subjects therefore consists of all the determined common components. The components that are filtered out as not common are merged with subspace \mathcal{Y}_{II} to form a new set of SCVs to identify subgroups of datasets that have more highly interfered components through an unsupervised analysis.

C. Data and Code Availability

The data that supports the findings of this study is openly available on the collaborative informatics and neuroimaging suite (COINS) data exchange repository (<https://coins.trendscenter.org/>). The codes used in this work are available upon direct request from the corresponding author. The data and code sharing adopted by the authors comply with the requirements of the funding bodies.

IV. RESULTS AND DISCUSSION

A. Simulations

We use IVA-G with a block Newton update that provides desirable convergence properties ([32]), and in what follows, demonstrate its effectiveness in subspace extraction.

1) *Simulation Setup*: To study the ability of IVA to maintain the structure of SCVs to effectively identify the subspaces, we design a set of simulations. Our application is fMRI data analysis and the latent fMRI sources are likely to be super-Gaussian distributed ([47]). Therefore, all the SCVs are generated from an MGGD with the shape parameter β randomly selected from the interval $[0.1, 0.8]$, which generates super-Gaussian marginals. The SCVs are mixed by randomly generated mixing matrices, $\mathbf{A}^{[k]}$, from a standard uniform distribution to form the datasets using (1). A total of $N = 30$ SCVs are generated with $V = 10000$ voxels and $K = 20$ datasets. Note that all the MGGD sources are normalized to zero mean and unit variance hence the covariance values and correlation (coefficients) coincide. These SCVs are grouped to imitate three subspaces and the details are as follows:

- The first group of 14 SCVs are simulated as common sources with high correlation value ρ_c . The correlation matrix of a common SCV is shown in Figure 3(a).
- The second group of 6 SCVs have structured correlation matrices with some higher value of ρ_c and some lower value of ρ_d . This indicates that the sources with higher correlation values are common within a subgroup of datasets. The structured correlation matrices are shown in Figure 3(b)–(g).
- The last group of 10 SCVs are simulated as distinct sources with low correlation value ρ_d . Figure 3(h) shows the correlation matrix of a distinct SCV.

Different cases are studied in the simulation with different values of ρ_c and ρ_d : Case 1, $\rho_c = 0.9, \rho_d = 0.1$, Case 2, $\rho_c = 0.8, \rho_d = 0.2$, Case 3, $\rho_c = 0.7, \rho_d = 0.3$, and Case 4, $\rho_c = 0.6, \rho_d = 0.4$.

2) *Simulation Results*: Figure 3 shows the correlation matrices of the true SCVs and the estimated SCVs for a random run for Case 1. To demonstrate that IVA identification condition enables preserving the structure of SCVs compared to MCCA due to its identification condition, we perform IVA-G and three versions of MCCA, *i.e.*, MCCA-GENVAR, MCCA with MAXVAR cost function (MCCA-MAXVAR), and MCCA with SSQCOR cost function (MCCA-SSQCOR), on the mixtures of sources, \mathbf{X} . MCCA-MAXVAR and MCCA-SSQCOR behave similar to MCCA-GENVAR and Figure 3 shows the results of IVA-G and MCCA-GENVAR. Both IVA-G and MCCA-GENVAR successfully extract the common subspace spanned by SCVs 1–14. But for the SCVs 15–20, as we can see there are only a subset of components highly correlated with each other. It is possible for some components in one SCV to have a certain level of correlation with the components in another SCV. MCCA-GENVAR estimates one SCV by maximizing the correlation among the sources across datasets. MCCA tends to group as many correlated sources as possible in the SCVs that are estimated first, due to its deflationary nature. Hence we observe some SCVs that are merged

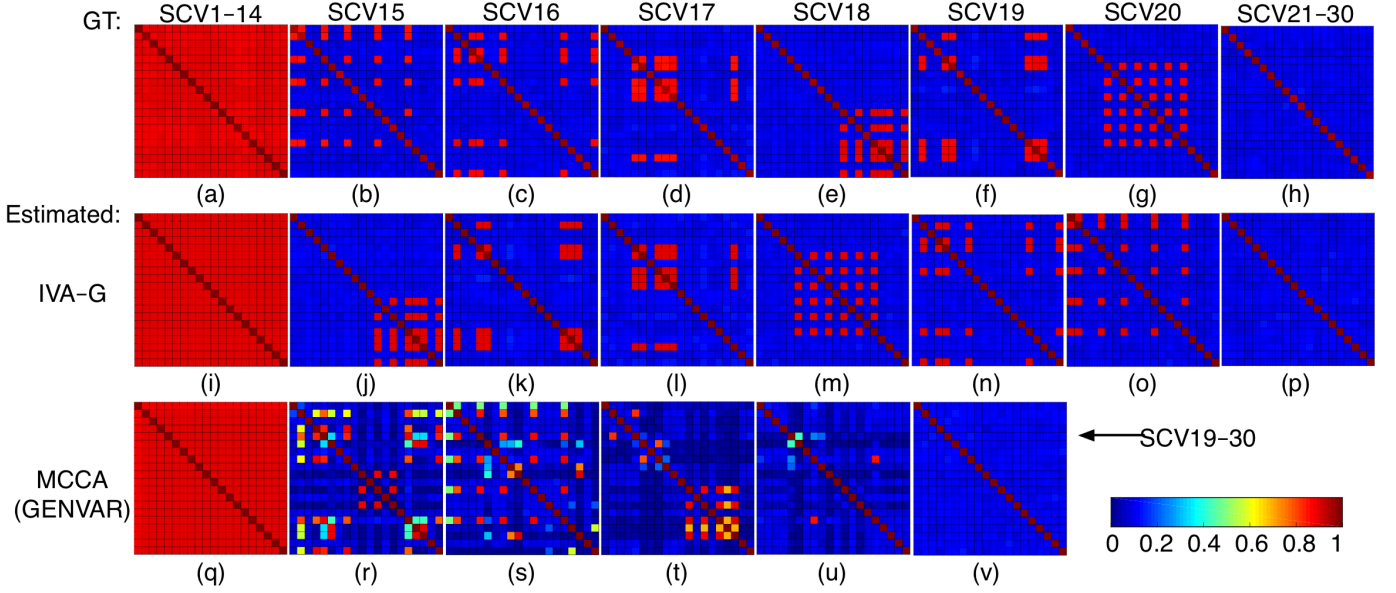


Fig. 3: Correlation matrices of true SCVs (a)–(h) and the estimated ones from IVA-G (i)–(p) and MCCA-GENVAR (q)–(v) in simulation. GT means ground truth.

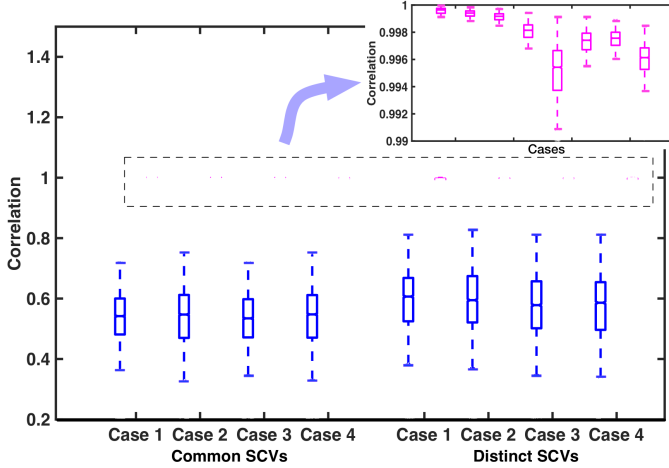


Fig. 4: Boxplots of the correlation values between the estimates and the ground truth for IVA-G in blue and IVA-L-SOS in magenta for the four cases. Statistics are calculated from 100 independent runs with different initialization. The box plot displays the median, the 25th and 75th percentiles of the correlation values with whiskers extending to the 99.3% confidence interval using the default settings.

together, as shown in Figure 3(r)–(u), and that the SCV15 and SCV16 contain more correlated sources than SCV17 and SCV18. This breaks the structure of true SCVs and makes it impossible to identify the subgroups of sources within an SCV, *i.e.*, to identify subspaces. As a result, MCCA yields fewer SCVs with structured correlation matrix and more distinct SCVs compared with the ground truth. In contrast, IVA-G successfully preserves the structure of all SCVs. Note that these SCVs are estimated subject to permutation ambiguity due to the nature of all blind source separation algorithms. This illustrates the desirable use of IVA-G to extract subspaces to identify subgroups.

3) *IVA-G and IVA-L-SOS*: Identification condition of IVA-G implies that IVA-G is not able to separate α -SCVs that have proportional correlation matrices no matter which distribution the latent sources are drawn from. The unseparable sources can be the whole SCVs or a subset of sources in the SCVs since $0 \leq K_\alpha \leq K$. In our simulation SCVs 1–14 have the same correlation matrix hence IVA-G identifies the whole subspace successfully while not the individual SCVs. The same situation for SCVs 21–30. As noted in Section II-B, an IVA algorithm that takes both SOS and HOS into consideration like IVA-L-SOS can solve this problem. We can either perform IVA-L-SOS on the original datasets or perform a secondary IVA-L-SOS decomposition on the subspace identified by IVA-G. Reliably identifying subspaces of interest by IVA-G followed by a secondary decomposition of an IVA algorithm that takes both SOS and HOS (and hence is computationally more complex) into consideration on the subspaces helps save considerable computation time. This two-step procedure guarantees better performance by first identifying a desirable starting point. This strategy is favorable in the applications of blind source separation and is the core in the common practice of performing principal component analysis first to provide an orthogonal initialization for an ICA decomposition.

The correlation between the estimates and the ground truth is calculated to evaluate the performance. IVA-G yields good estimation of SCV15–20 and their average correlation is 0.996 ± 0.014 across all four cases. To explore the ability of IVA-L-SOS to separate α -SCVs with proportional correlation matrices, a secondary IVA-L-SOS decomposition is performed on the common and distinct subspace separately. The common and distinct subspaces are constructed separately by multiplying the common and distinct SCVs from IVA-G with their associated mixing matrices calculated as the inverse of the estimated demixing matrices. Figure 4 shows that IVA-G yields common components that are not highly correlated with the ground truth. However, these components are very reliably

estimated by the secondary IVA-L-SOS with correlation values close to 1. This verifies that the identification issue of IVA is not a problem anymore when HOS is taken into consideration.

B. Application to Multi-subject Resting State fMRI Data

1) *Data Acquisition and Preprocessing*: The data used in this study is a resting state fMRI data from the Center of Biomedical Research Excellence (COBRE), which is available on the collaborative informatics and neuroimaging suite data exchange repository (<https://coins.trendscenter.org/>) ([48]–[50]). The data includes 88 SZs (average age: 37 ± 14) and 91 HCs (average age: 38 ± 12). For this study, the participants were asked to keep their eyes open during the entire scanning period. All images were collected on a single 3-Tesla Siemens Trio scanner with a 12-channel radio frequency coil using the following parameters: TE = 29 ms, TR = 2 s, flip angle = 75° , slice thickness = 3.5 mm, slice gap = 1.05 mm, voxel size $3.75 \times 3.75 \times 4.55 \text{ mm}^3$. Participants were instructed to keep their eyes open during the scan and stare passively at a central fixation cross. Each resting state scan consists of 150 volumes. To eliminate the T1-related signal fluctuations (T1 effect) ([51]), the first 6 volumes are removed in this study, thus 144 volumes remain for each subject. The fMRI data are realigned with INRIalign algorithm ([52]), slice-timing correction is applied using the middle slice as the reference frame in the functional data pipeline and spatially normalized to the standard Montreal Neurologic Institute (MNI) space ([53]) and resampled to $3 \times 3 \times 3 \text{ mm}^3$, resulting in $53 \times 63 \times 46$ voxels. Afterwards, the fMRI data are smoothed using a Gaussian kernel with a full-width at half-maximum of 5 mm.

2) *Parameter Selection*: IVA procedure we employ does not require the selection of any parameter except the model order, *i.e.*, the dimension of signal space N . However, for fMRI data, classical order estimation techniques based on information theoretic criteria may overestimate the order due to the inherent sample dependence of fMRI data ([54], [55]). A common way to overcome this issue is by using downsampling to obtain effectively independent and identically distributed samples ([54], [55]). However, methods based on downsampling suffer from a loss of information associated with it. More recently, two entropy rate (ER)-based order estimation techniques are proposed that account for sample dependence without the use of downsampling: ER using a finite memory length model (ER-FM) and ER using an autoregressive model (ER-AR) ([56]). Since the sample correlation structure in ER-FM is a better match to that in fMRI data due to the finite span of correlation in the point spread function, ER-FM is used in this paper to estimate the order of signal space for each subject. The final value of N is selected as the mean plus one standard deviation of the orders computed across all the subjects and is fixed for the IVA decompositions on R subsets. The mean and standard deviation of the order across subjects are 72.86 ± 10.40 . We use an order equal to the mean plus one standard deviation, which is rounded up to 85 to retain a significant level of the variability across multiple subjects while introducing minimal noise. The use of this high model order is also well motivated in the literature for achieving a

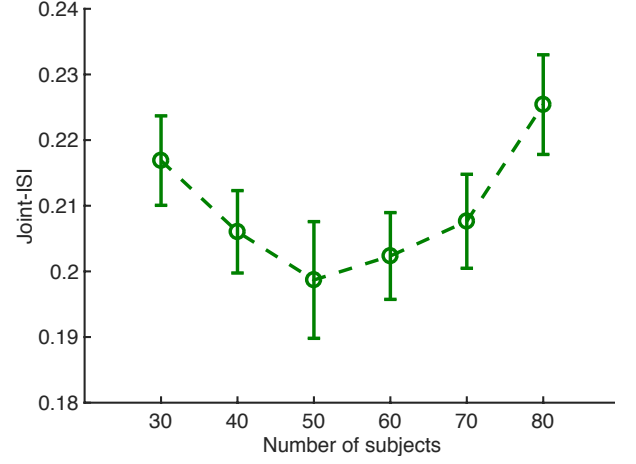


Fig. 5: Plot of joint-ISI as a function of the number of subjects when performing IVA-G on the hybrid data. The mean and standard deviation calculated from the results of 20 runs are shown.

more useful functional segmentation of the brain, see *e.g.*, ([37], [38]). The dimension of each dataset is reduced to 85 by performing a principal component analysis.

To achieve a reliable IVA decomposition, we need sufficient number of samples per estimated parameter so that IVA can effectively take dataset dependence into account. The performance of IVA degrades as the number of datasets, K , or the number of sources, N , increases beyond a certain point, when number of samples, V , is fixed. The estimation of the source covariance matrix that determines the multivariate Gaussian distribution of each SCV is required in IVA-G for each update of demixing matrices \mathbf{W} , which in turn is used to estimate the SCVs. The total number of samples in a dataset is $NV \times K$. The number of free parameters to be estimated in the covariance matrix for each of K SCVs is $\frac{K(K-1)}{2}$. Hence the number of samples per free parameter is $\frac{NV \times K}{N \times \frac{K(K-1)}{2}} = \frac{2V}{K-1}$, which is inversely proportional to K . When updating the demixing matrices \mathbf{W}_k , there are KN^2 free parameters hence the number of samples per free parameter is $\frac{NV \times K}{KN^2} = \frac{V}{N}$, which is inversely proportional to N . To explore the optimal value of K that balances the effect of high dimensionality and maximal subject information when the N is fixed—*i.e.*, determined using a data-driven approach—we design a hybrid simulation. The estimated 85 COBRE sources as presented in our previous study ([57]) are used as the sources and mixed by the randomly generated mixing matrices to produce the hybrid data. With a fixed model order and a fixed number of voxels, the number of subjects K is changed from 30 to 80 with increments of 10. The performance is measured by joint-ISI which is defined as

$$\text{ISI}_{\text{JNT}}(\mathbf{G}^{[1]}, \mathbf{G}^{[2]}, \dots, \mathbf{G}^{[K]}) \triangleq \text{ISI} \left(\frac{1}{K} \sum_{k=1}^K |\mathbf{G}^{[k]}| \right), \quad (11)$$

where

$$\text{ISI}(\mathbf{G}) = \frac{1}{2N(N-1)} \cdot \sum_{n=1}^N \left(\frac{\sum_{m=1}^N \|g_{nm}\|}{\max_p \|g_{np}\|} - 1 \right) + \frac{1}{2N(N-1)} \cdot \sum_{m=1}^N \left(\frac{\sum_{n=1}^N \|g_{nm}\|}{\max_p \|g_{pm}\|} - 1 \right) \quad (12)$$

and $\mathbf{G}^{[k]} = \mathbf{W}^{[k]} \mathbf{A}^{[k]}$ with elements denoted as g_{nm} ([58]). $\mathbf{A}^{[k]}$ is the true mixing matrix and $\mathbf{W}^{[k]}$ is the estimated demixing matrix. If $\mathbf{W}^{[k]}$ is perfectly estimated, $\mathbf{G}^{[k]}$ is identity subject to permutation and scaling ambiguities, thus yielding zero ISI that indicates a perfect separation. Therefore, the smaller the joint-ISI, the closer the estimates are to the ground truth.

From Figure 5 we see that the performance of IVA-G improves with increase in the number of datasets until a certain value of K , after which the performance degrades. This illustrates that when the number of datasets used in an IVA decomposition is too small, the interaction information across datasets is not sufficient for an accurate estimation of the sources. Hence the performance improves with more number of datasets. However, for a larger number of datasets, IVA suffers from the curse of dimensionality. Thus, the performance degrades. The experimental results show that there indeed exists an optimal value of the number of datasets for an IVA decomposition that balances the requirement of interaction information and the dimensionality issue. The optimal number of subjects in this application is determined as $K = 50$, where IVA yields the best performance, *i.e.*, the lowest joint-ISI as shown in Figure 5. This value is then used as the subset size in subset analysis of IVA-G-CS. We randomly selected five subsets of subjects for each group to ensure that each subject is included at least once in the decompositions. Note that in this work the values of all dimension parameters are determined in a data-driven manner.

3) Common Subspace Identification Using IVA-G-CS:

IVA-G-CS is applied to SZ group and HC group separately to identify their subspaces. Five subsets of 50 subjects are randomly selected for each group and 85 SCVs are estimated from each subset. The value at each voxel of the estimated source is transformed into Z -scores before any calculation of metrics hence the covariance and correlation coincide. For each SCV, there are $50 \times (50 - 1)/2 = 1225$ distinct correlation values. The smoothed distribution of correlation values is plotted as a function of the index of SCVs for the fifth subset of SZs and the second subset of HCs as shown in Figure 6. The similar plots of the other subsets are provided as supplementary materials. The SCVs are sorted by the mean value of correlation to roughly order them from high correlation to low correlation. From Figure 6(a) we can see there is a group of SCVs with all their correlation values higher than 0.2. Using $\sigma_t^2 = 0.2$, the commonality q and dissimilarity \tilde{q} are calculated and plotted in yellow and purple, respectively. In the application to this dataset, we chose $\delta_1 = 0.98$ and $\delta_2 = 0.02$. More than 90% of the first 28 SCVs have $q \geq 0.98$ and $\tilde{q} \leq 0.02$ in the fifth subset of SZs. This suggests that the first 28 SCVs are common across the subjects in this subset. Finally, the numbers of common

SCVs M_r for all five subsets of SZ group are determined as 23, 30, 33, 35, 28, respectively. For HC group, the numbers are 31, 32, 28, 34, 34, respectively. The number of candidates, M , in the subspace \mathcal{Y}_{r-1} is determined as 35, which is the largest one among the ten values. The 25th percentile of the cross-correlation values of the M candidates is used as threshold t for the identification of common components. Each identified common component is consistently estimated in at least 80% of the subsets. Note that the values of σ_t^2 , δ_1 , and δ_2 are selected such that the average correlation values in the subspaces are as different as possible. Determining the value of M as the largest one across multiple subsets mitigates the sensitivity of the choice of parameters by allowing more candidates available for common component identification.

a) Artifact Removal: Using the common component identification method presented in Section III-B, 25 and 24 common components are determined for SZ and HC groups separately. Among the determined common components, some of them have high ventricle effects and hence should be removed from further analysis. We utilize the grey matter (GM) and cerebrospinal fluid (CSF) MNI templates included in SPM 12 to distinguish the components ([59], [60]). The correlation between the common components and the two templates, C_{GM} and C_{CSF} , are calculated. Each component is normalized to Z -score and thresholded by $Z = 2$ which means that the voxels with $Z < 2$ are set to zero. The components are divided into two groups with respect to the median value of $C_{\text{GM}} - C_{\text{CSF}}$. The components in the first group are with $C_{\text{GM}} - C_{\text{CSF}}$ higher than the median hence they are more likely to be RSNs and those in the second group are more likely to be ventricle effects. To ensure all the RSNs are retained and the ventricle effects are removed, we further do a visual check. The grouping by the correlation reduces the burden of a visual check. The median value of $C_{\text{GM}} - C_{\text{CSF}}$ is 0.18 for SZs and 0.22 for HCs. Finally, 14 common RSNs are obtained for SZs and 16 for HCs after artifact removal. The average correlation values of the 14 common RSNs of SZs is 0.66 ± 0.15 and that of the 16 common RSNs of HCs is 0.68 ± 0.10 .

The identified common components of each group are typical RSN components like those found in previous studies ([37], [38]). They are grouped into six domains, motor, cognitive control (COG), default mode (DM), auditory (AUD), visual (VIS) and cerebellum (CB), according to their anatomical and presumed functional properties as in ([38]). Figure 7 shows the composite spatial maps for each cluster. The results show that two common components of SZs include two different interesting RSNs, the first one merges the motor cortex (precentral and postcentral gyrus) and the auditory cortex (superior temporal gyrus) and the other one merges the precuneus gyrus and the right frontoparietal network. The merging of two different RSNs into a single source component does not occur in the HC group. This observation suggests a high correlation between these RSN pairs might result from decreases in connectivity in the brain of individuals with schizophrenia ([61]–[63]) hence more networks are involved in its functioning.

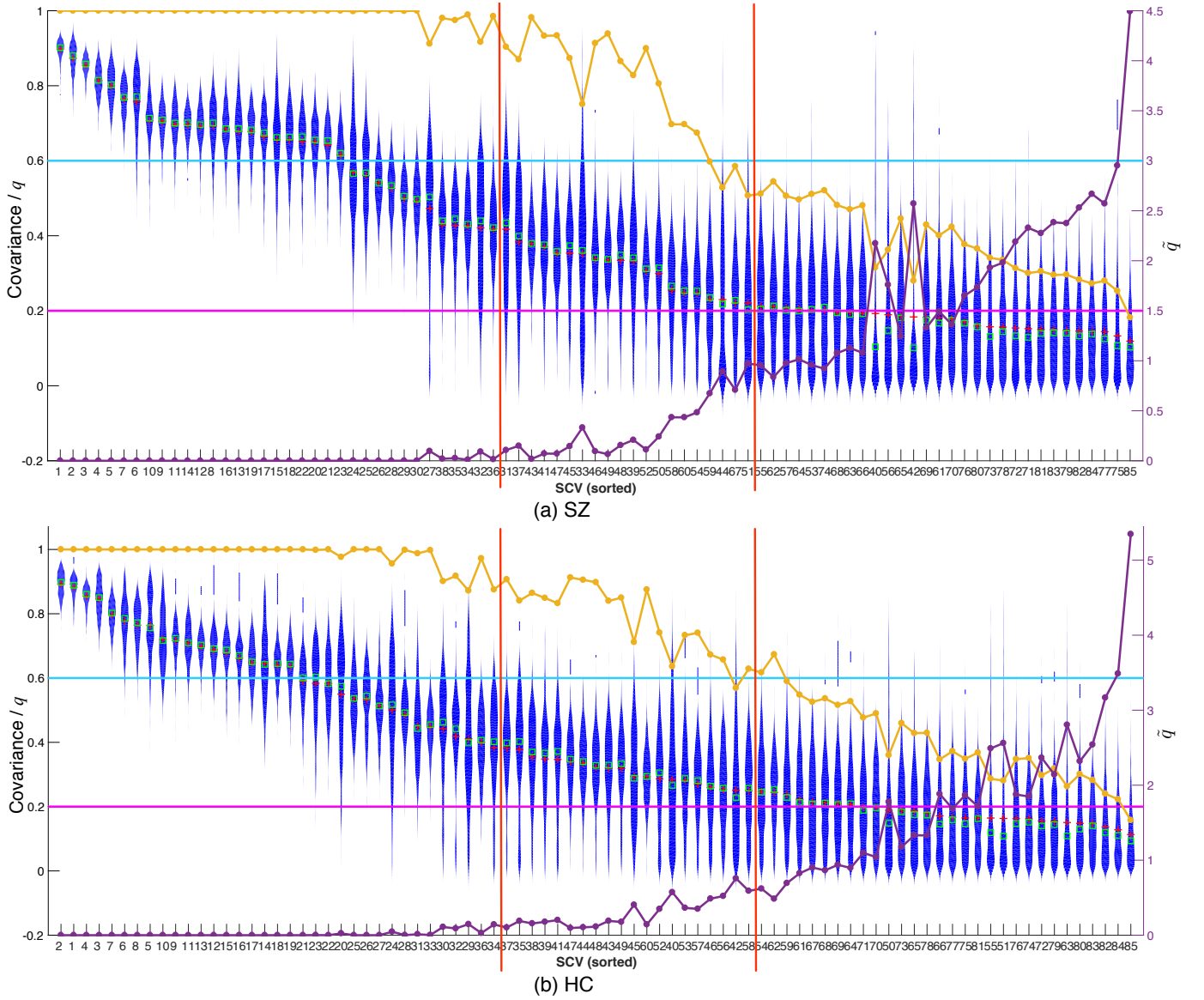


Fig. 6: Smoothed distribution of the correlation values of the fifth subset of SZs (a) and the second subset of HCs (b). The red crosses and the green squares denote the mean and median. Two ratios q and \tilde{q} are plotted in yellow and purple. Two vertical red lines denotes the margins between different groups of SCVs. Blue and magenta horizontal lines denotes 0.6 and 0.2 which are used for a comparison of the three groups of SCVs.

4) *Analysis of Group-specific SCVs:* From the violin plots in Figure 6, we can identify two more subspaces, \mathcal{Y}_{II} and \mathcal{Y}_{III} (distinct subspace). The subspace \mathcal{Y}_{II} has a mix of both high and low correlation values and \mathcal{Y}_{III} has very low correlation values. The value of P that is used to determine the subspace \mathcal{Y}_{II} is set as 40. Further analysis of these two groups is of interest as well. The SCVs in subspace \mathcal{Y}_{II} are called group-specific SCVs since they suggest that the components from some subgroups of subjects have higher correlation hence can be used to identify those subgroups. As we know that the brain functions differently in patients of schizophrenia compared with HCs. Using the group-specific SCVs, we seek to identify subgroups of patients that have RSNs with significant correlation which may result from similar functional patterns. The results indeed show that

the subgroups identified using group-specific SCVs reflect similarity within each subgroup and significant differences across subgroups in terms of the spatial activation patterns of their RSNs. We also conduct statistic test on their clinical symptoms that are scored by PANSS and discover differences with certain significance level.

From the distribution plots of correlation values shown in Figure 6(a), the subspace \mathcal{Y}_{II} is determined as that located within two vertical red lines. Meanwhile, those SCVs that are filtered out by common subspace identification are treated as group-specific SCVs as well. Consequently, $N_G = 30$ group-specific SCVs are identified for SZs. A k-means clustering is performed on the correlation matrices of the group-specific SCVs to find out clusters that have similar correlation matrices to help identify source components that are common within

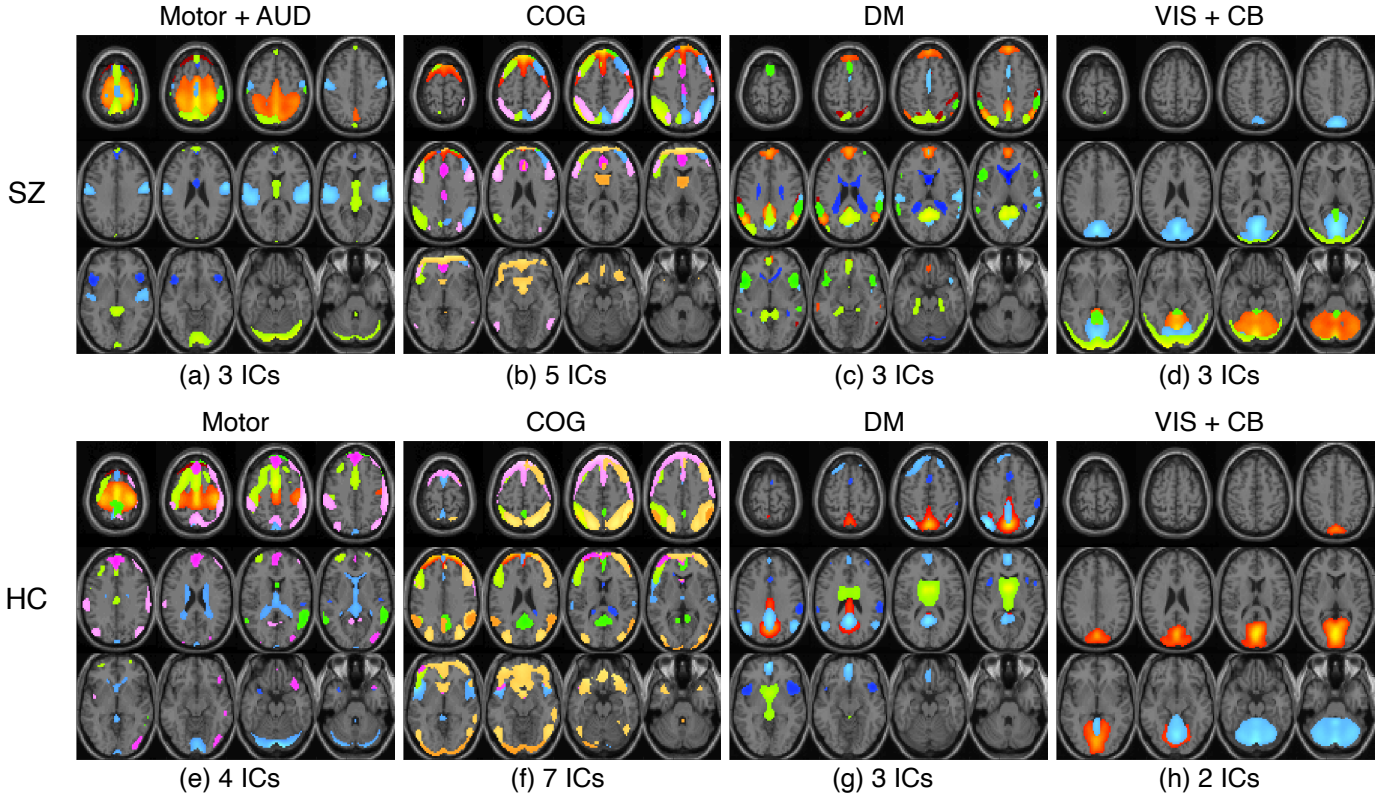


Fig. 7: Spatial maps of the common components in six categories: Motor; COG, cognitive control; DM, default mode; AUD, auditory; VIS, visual; CB, cerebellum. (a)-(d) for SZ group and (e)-(h) for HC group. The number of independent components (ICs) that are composited in each subfigure is listed and different colors refer to the spatial maps of individual components. The anatomical regions of the activation in the common components are provided in the supplementary materials.

the same subgroup of subjects. The mean correlation matrix of a cluster is used to identify the subgroups of subjects. As shown in Figure 8(c) and (d), the mean correlation matrix is rearranged to assemble the subgroup modules by maximizing the modularity of the matrix, which is called modularization. Modularity is a measure that quantifies the community structure of a network that is summarized in a matrix ([64]). As shown in Figure 8(c), two clusters with higher modularity, 0.39 and 0.21, each yields three separate clear subgroups. There is no significant difference associated with age among the subgroups ($p \geq 0.1541$).

To compare the spatial activation patterns of the RSNs across subgroups in each cluster, we perform a two-sample t -test on the activation value at each voxel of the spatial map across the subjects within each subgroup. False discovery rate (FDR) correction is conducted throughout all comparisons and the associated confidence interval after FDR correction is reported. Cluster I includes three components and two of them show significant differences in spatial activation patterns, as shown in Figure 8(d). Subgroup 1 yields higher activation in the posterior cingulate gyrus and Brodmann area (BA) 31, and lower activation in the secondary visual cortex compared with subgroups 2 and 3. Subgroup 2 has lower activation than the other two subgroups in the anterior and posterior cingulate gyrus. Cluster II includes five components and three of them show significant differences in spatial activation patterns, as shown in Figure 8(e). Subgroup 3 has lower activation in the

primary somatosensory and motor cortex, and higher activation in the secondary visual cortex. Subgroup 2 has lower activation in angular gyrus and higher activation in the inferior frontal gyrus. A particular case is the very small area of activation in BA30 that shows significant differences with 100% confidence interval after FDR correction between subgroups 1 and 3.

A multivariate analysis of variance (MANOVA) is conducted on five statistics—mean, standard deviation, median, minimum, and maximum—of all the thirty PANSS scores ([39]) including seven positive, seven negative, and sixteen general scales. The MANOVA yields in F -score=3.978 ($p = 6.816 \times 10^{-5}$) that demonstrates significant differences across the three subgroups in Cluster I (Cluster II was not significant). Figure 9 summarizes the dominant and absent symptoms of each subgroup. The dominant symptoms of a subgroup refer to those that have median value greater than 2 or the median value is 2 for one subgroup while is 1 (which means absent) for the other two subgroups. In Cluster I, as shown in Figure 9(b), subgroup 3 has more dominant symptoms, subgroup 2 has more absent symptoms, and subgroup 1 has obvious broader range for a number of symptoms such as delusions, tension, lack of judgment and insight, and active social avoidance. In Cluster II, as shown in Figure 9(d), all three subgroups have several dominant symptoms. Subgroup 2 has more absent symptoms and subgroup 3 has broader range for symptoms such as stereotyped thinking, anxiety,

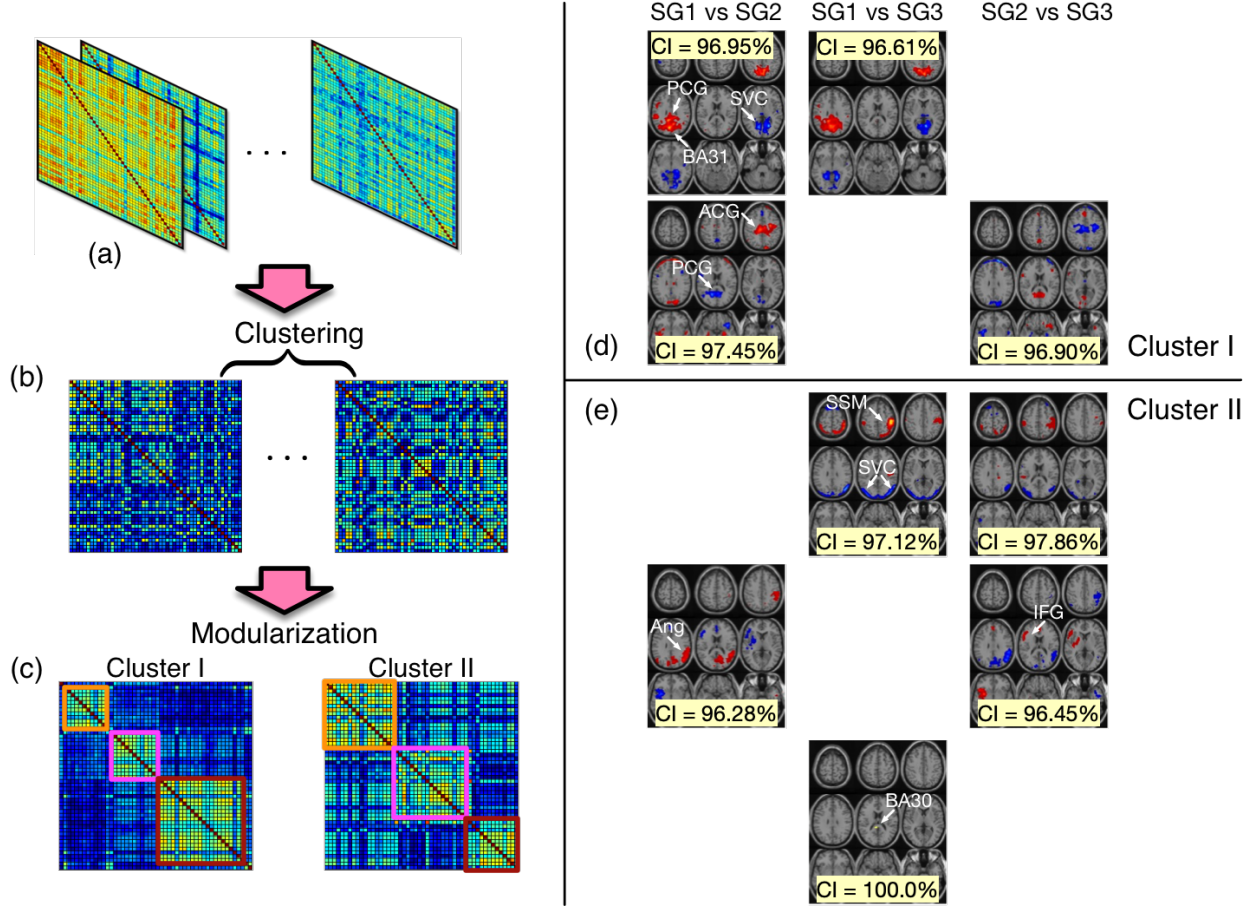


Fig. 8: The clustering and modularization processes of the correlation matrices of group-specific SCVs and the two clusters that yield clear subgroups of patients (a-c). Subgroup 1, 2, and 3 are labeled by orange, magenta, and red squares separately. The differences of spatial activation patterns across subgroups in Cluster I (d) and Cluster II (e) are represented by the t -statistic from a two sample t -test with FDR (≤ 0.05) control and the associated confidence interval (CI) is reported. The brain regions that show significant subgroup (SG) differences including: posterior cingulate gyrus (PCG), BA31, secondary visual cortex (SVC), anterior cingulate gyrus (ACG), primary somatosensory and motor cortex (SSM), angular gyrus (Ang), inferior frontal gyrus (IFG), and BA30.

and tension. All subgroups possess their unique dominant and absent symptoms. We also conduct a MANOVA on the symptoms present in all three subgroups. The MANOVA detects significant differences among the subgroups in Cluster I with F-score=4.1367 ($p = 8.302 \times 10^{-5}$). In Cluster II, only the standard deviation demonstrates significant differences among subgroups with F-score=3.3846 ($p = 0.0404$).

V. DISCUSSION

Through the investigation of spatial activation patterns of the networks across subgroups, we find several interesting networks that show significant subgroup differences. Most of the networks such as the cingulate gyrus ([65]), somatosensory and motor cortex ([66]), angular gyrus, inferior frontal gyrus ([67]), and secondary visual cortex ([68]) are reported to be related to schizophrenia ([69], [70]). One particular case is the third component in Cluster II because the activated region that shows significant differences between two subgroups is very small yet very interesting. This network is BA30 which does not have a specific name and only the function of its left

part, where the activation pattern shows significant subgroup differences, is reported in ([71], [72]). Its function is related to attending to speech and listening to sentences. Hearing voices is the most common type of hallucination—one of the typical symptoms—in people with schizophrenia.

In addition to studying the differences across the identified subgroups using the spatial maps of the networks extracted from fMRI data, we also investigate the differences in terms of their clinical data—PANSS scores. PANSS scores—1 means absent and 7 means extreme—are medical scales used for measuring symptom severity of patients with schizophrenia ([39]). The self-reported symptom scores are, in general, subjective and noisy, and hence not effective in terms of categorization of disease. Focusing the analysis on individual PANSS scores is not sufficient to describe the subgroups. By investigating the PANSS scores via a MANOVA, we find significant differences across the subgroups and identify unique dominant and absent symptoms for each subgroup. The high significance level provides more confidence in the identified subgroups in Cluster I. Extracting reliable information of the

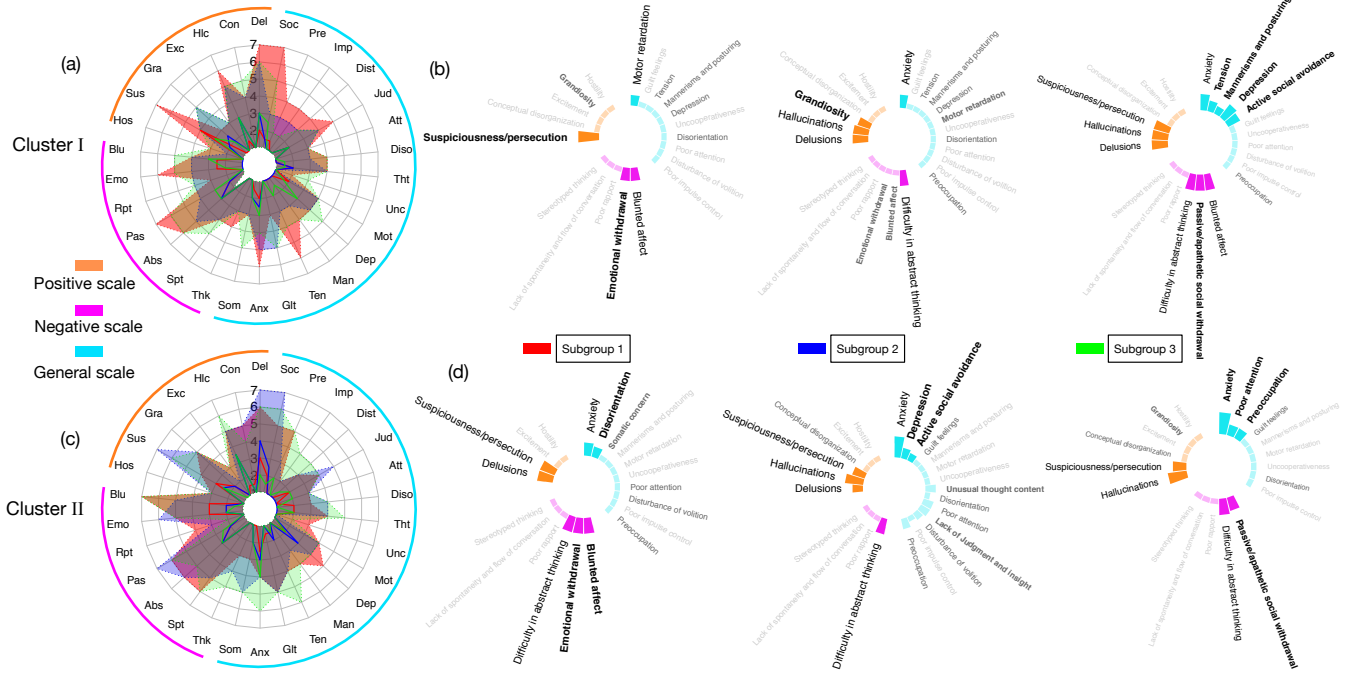


Fig. 9: The median (connected by solid lines), minimum, and maximum (connected by dash lines) values of each PANSS score of subgroups in Cluster I (a) and Cluster II (c), and the dominant (bright orange, magenta, and cyan) and absent (fade orange, magenta, and cyan) symptoms of each subgroup in Cluster I (b) and Cluster II (d). In (b) and (d), the bold symptoms refer to those that are unique for a subgroup and the translucent symptoms refer to those that are absent from all three subgroups.

subgroups of schizophrenia from both the neuroimaging data and clinically diagnostic data can potentially lead to a better understanding of the underlying heterogeneity of the disorder and in the future may lead to improved categorization and treatment strategies.

Along with the model order and the number of datasets to be used in a single IVA decomposition, which are determined in a data-driven manner, there are other parameters in the proposed procedure that are practically determined. However, these parameters are easy to determine and can be categorized into two classes. The first class includes the thresholds, the correlation threshold t and σ_t^2 . These can vary across different datasets but are easy to determine. For the value of t the suggestion is to use a simple statistic, such as the 25th percentile used in this work, of all the correlation values. Two examples of the correlation structure analysis are shown in Figure 6, where we clearly see the three distinguishable subspaces. This demonstrates the strength of IVA-CS to identify subspaces. Hence in cases where there are distinguishable subspaces the threshold σ_t^2 needed for further division is also easy to determine. Thresholding method might not be effective in cases where the subspaces are not clearly delineated. A better choice of the division of subspaces in these scenarios can be achieved by using additional meaningful prior information such as sparsity that is used in ([73]). However, in most cases, the groups are heterogeneous and we would expect to see such subspace clusters. The other class of parameters includes parameters such as, 80% of the subsets, δ_1 , δ_2 , and the percentage of group-specified components, P . These are ratios that are practically determined to be large or small enough to

avoid missing useful information or including unreliable, noisy information. Their determination depends on users' choice. Small changes in these ratios are not expected to change the conclusions. Furthermore, the parameters included in the second stage and post analysis do not influence the use of IVA-CS for subspace analysis in other applications since the proposed flexible framework allows researchers to design their own way of extracting information from the subspaces. Hence the parameters can be either accordingly reserved for easy selection or fully omitted due to the design of experiment.

VI. CONCLUSION AND FUTURE DIRECTIONS

Given the importance of common and distinct subspace analysis in medical imaging data analysis, a number of recent studies had a focus on this aspect, in particular for fusion of different modalities or tasks where only a couple of datasets are jointly analyzed. However, joint analysis of large-scale medical imaging data such as multi-subject fMRI data collected from tens, or typically hundreds of subjects enables one to leverage the rich information across the datasets. Here, we introduced a new method called IVA-CS to extract subspaces from at least a hundred of datasets by leveraging the strength of IVA in identification through successful preservation of the complete SCV structure. This allows for efficient identification and estimation of subspaces by carefully studying the dependence structure of SCVs. IVA-CS also mitigates the high dimensionality issue of IVA by introducing subset analysis to determine a desirable number of datasets that is high enough to exploit the dependence across datasets and is not affected by issues regarding high dimensionality. The simulation study

verifies the ability of IVA to preserve subspace structure and its application to real fMRI data demonstrates its effectiveness. The identified common components with two linked networks provide evidence of the functional dysconnectivity in the brain of SZs. A subspace of group-specific SCVs is identified by IVA-CS for the SZ group as well. The subgroups of SZ recognized using the group-specific SCVs exhibit significant differences in terms of their brain networks as well as their clinical symptoms that are measured by PANSS. These findings emphasize the importance of interpreting subtypes of schizophrenia in terms of both the neuroimaging data analysis and the clinically diagnostic data. A better understanding of the underlying heterogeneity of the disorder in the future may lead to improved categorization and treatment strategies.

IVA-CS successfully identifies subspaces for the COBRE dataset where we demonstrated its robustness through a subset analysis. It will be desirable to apply IVA-CS to different datasets to provide further evidence that the proposed framework is useful. Other interesting future directions include the use of common components estimated by IVA-CS. They represent the global information of the population of a group hence allowing for the identification of more reliable and robust brain patterns of the patients with mental disorder. In the application to the analysis of fMRI data that is collected from at least a hundred of subjects, we demonstrate that IVA-G—an IVA algorithm that uses only SOS—reliably extracts interpretable common RSNs that are consistent with previous work. In this work, we use subset analysis to mitigate the high dimensionality issue. As discussed in [33], another way to deal with the high dimensionality issue of IVA is to use constrained IVA ([74])—a semi-blind source separation technique—to shrink the solution space. The common components from IVA-G-CS hence can be used as constraints to mitigate the high dimensionality issue and to guide the analysis with an IVA algorithm that uses both SOS and HOS. One other possible future application is the dynamics study of brain function using fMRI data, where each dataset is further divided into multiple datasets thus resulting in hundreds even thousands of datasets.

ACKNOWLEDGMENT

This work was supported by NSF-CCF 1618551, NSF-NCS 1631838, NSF 1539067 and NIH grants R01MH118695, R01EB020407, R01EB006841, P20GM103472, and P30GM12 2734. The authors thank the research staff from the Mind Research Network COBRE study who collected, preprocessed and shared the data. The authors appreciate the valuable feedback provided by the members of Machine Learning for Signal Processing Laboratory in University of Maryland, Baltimore County.

The hardware used in the computational studies is part of the UMBC High Performance Computing Facility (HPCF). The facility is supported by the U.S. National Science Foundation through the MRI program (grant nos. CNS-0821258, CNS-1228778, and OAC-1726023) and the SCREMS program (grant no. DMS-0821311), with additional substantial support from the University of Maryland, Baltimore County (UMBC). See hpcf.umbc.edu for more information on HPCF and the projects using its resources.

REFERENCES

- [1] M. E. Shenton, R. Kikinis, F. A. Jolesz, S. D. Pollak, M. LeMay, C. G. Wible, H. Hokama, J. Martin, D. Metcalf, M. Coleman *et al.*, “Abnormalities of the left temporal lobe and thought disorder in schizophrenia: A quantitative magnetic resonance imaging study,” *New England Journal of Medicine*, vol. 327, no. 9, pp. 604–612, 1992.
- [2] R. D. Pascual-Marqui, D. Lehmann, T. Koenig, K. Kochi, M. C. Merlo, D. Hell, and M. Koukkou, “Low resolution brain electromagnetic tomography (LORETA) functional imaging in acute, neuroleptic-naïve, first-episode, productive schizophrenia,” *Psychiatry Research: Neuroimaging*, vol. 90, no. 3, pp. 169–179, 1999.
- [3] R. E. Gur, P. E. Cowell, A. Latshaw, B. I. Turetsky, R. I. Grossman, S. E. Arnold, W. B. Bilker, and R. C. Gur, “Reduced dorsal and orbital prefrontal gray matter volumes in schizophrenia,” *Archives of General Psychiatry*, vol. 57, no. 8, pp. 761–768, 2000.
- [4] S. Ma, V. D. Calhoun, R. Phlypo, and T. Adali, “Dynamic changes of spatial functional network connectivity in healthy individuals and schizophrenia patients using independent vector analysis,” *NeuroImage*, vol. 90, pp. 196–206, 2014.
- [5] V. Abolghasemi, S. Ferdowsi, and S. Sanei, “Fast and incoherent dictionary learning algorithms with application to fMRI,” *Signal, Image and Video Processing*, vol. 9, no. 1, pp. 147–158, 2015.
- [6] A. Jablensky, “Subtyping schizophrenia: implications for genetic research,” *Molecular Psychiatry*, vol. 11, no. 9, p. 815, 2006.
- [7] —, “The diagnostic concept of schizophrenia: Its history, evolution, and future prospects,” *Dialogues in Clinical Neuroscience*, vol. 12, no. 3, p. 271, 2010.
- [8] D. B. Dwyer, C. Cabral, L. Kambeitz-Illankovic, R. Sanfelici, J. Kambeitz, V. Calhoun, P. Falkai, C. Pantelis, E. Meisenzahl, and N. Koutsouleris, “Brain subtyping enhances the neuroanatomical discrimination of schizophrenia,” *Schizophrenia Bulletin*, vol. 44, no. 5, pp. 1060–1069, 2018.
- [9] J. F. Hallmayer, L. Kalaydjieva, J. Badcock, M. Dragović, S. Howell, P. T. Michie, D. Rock, D. Vile, R. Williams, E. H. Corder *et al.*, “Genetic evidence for a distinct subtype of schizophrenia characterized by pervasive cognitive deficit,” *The American Journal of Human Genetics*, vol. 77, no. 3, pp. 468–476, 2005.
- [10] D. Geisler, E. Walton, M. Naylor, V. Roessner, K. O. Lim, S. C. Schulz, R. L. Gollub, V. D. Calhoun, S. R. Sponheim, and S. Ehrlich, “Brain structure and function correlates of cognitive subtypes in schizophrenia,” *Psychiatry Research: Neuroimaging*, vol. 234, no. 1, pp. 74–83, 2015.
- [11] B. Morar, J. C. Badcock, M. Phillips, O. P. Almeida, and A. Jablensky, “The longevity gene Klotho is differentially associated with cognition in subtypes of schizophrenia,” *Schizophrenia Research*, vol. 193, pp. 348–353, 2018.
- [12] S. Senn, “Statistical pitfalls of personalized medicine,” *Nature*, vol. 563, pp. 619–621, 2018.
- [13] V. D. Calhoun and T. Adali, “Feature-based fusion of medical imaging data,” *IEEE Transactions on Information Technology in Biomedicine*, vol. 13, no. 5, pp. 711–720, Sep. 2009.
- [14] S. Ma, V. D. Calhoun, T. Eichele, W. Du, and T. Adali, “Modulations of functional connectivity in the healthy and schizophrenia groups during task and rest,” *NeuroImage*, vol. 62, no. 3, pp. 1694–1704, Sep. 2012.
- [15] J. Sui, T. Adali, Q. Yu, J. Chen, and V. D. Calhoun, “A review of multivariate methods for multimodal fusion of brain imaging data,” *Journal of Neuroscience Methods*, vol. 204, no. 1, pp. 68–81, 2012.
- [16] T. Adali, Y. Levin-Schwartz, and V. D. Calhoun, “Multi-modal data fusion using source separation: Application to medical imaging,” *Proceedings of the IEEE*, vol. 103, no. 9, pp. 1494–1506, 2015.
- [17] S. P. Ponnappalli, M. A. Saunders, C. F. Van Loan, and O. Alter, “A Higher-Order Generalized Singular Value Decomposition for Comparison of Global mRNA Expression from Multiple Organisms,” *PLoS ONE*, vol. 6, no. 12, pp. e28072+, Dec. 2011.
- [18] K. Van Deun, I. Van Mechelen, L. Thorrez, M. Schouteden, B. De Moor, M. J. van der Werf, L. De Lathauwer, A. K. Smilde, and H. A. Kiers, “DISCO-SCA and properly applied GSVD as swinging methods to find common and distinctive processes,” *PloS One*, vol. 7, no. 5, p. e37840, 2012.
- [19] E. F. Lock, K. A. Hoadley, J. S. Marron, and A. B. Nobel, “Joint and individual variation explained (JIVE) for integrated analysis of multiple data types,” *The Annals of Applied Statistics*, vol. 7, no. 1, p. 523, 2013.
- [20] A. Klami, S. Virtanen, and S. Kaski, “Bayesian canonical correlation analysis,” *Journal of Machine Learning Research*, vol. 14, no. Apr, pp. 965–1003, 2013.

- [21] Y. Levin-Schwartz, V. D. Calhoun, and T. Adalı, "Quantifying the interaction and contribution of multiple datasets in fusion: Application to the detection of schizophrenia," *IEEE Transactions on Medical Imaging*, vol. 36, no. 7, pp. 1385–1395, 2017.
- [22] K. Dontaraju, S.-J. Kim, M. Akhond, and T. Adalı, "Capturing common and individual components in fMRI data by discriminative dictionary learning," in *2018 52nd Asilomar Conference on Signals, Systems, and Computers*, 2018, pp. 1351–1356.
- [23] A. Iqbal, A.-K. Seghouane, and T. Adalı, "Shared and subject-specific dictionary learning (ShSSDL) algorithm for multisubject fMRI data analysis," *IEEE Transactions on Biomedical Engineering*, vol. 65, no. 11, pp. 2519–2528, 2018.
- [24] Y. Guo and L. Tang, "A hierarchical model for probabilistic independent component analysis of multi-subject fMRI studies," *Biometrics*, vol. 69, no. 4, pp. 970–981, 2013.
- [25] T. Kim, I. Lee, and T.-W. Lee, "Independent vector analysis: Definition and algorithms," in *Proc. of 40th Asilomar Conference on Signals, Systems, and Computers*, Oct. 2006, pp. 1393–1396.
- [26] T. Kim, T. Eltoft, and T.-W. Lee, "Independent vector analysis: An extension of ICA to multivariate components," in *Independent Component Analysis and Blind Signal Separation*, ser. Lecture Notes in Computer Science, J. Rosca, D. Erdogmus, J. Principe, and S. Haykin, Eds. Springer Berlin / Heidelberg, 2006, vol. 3889, pp. 165–172.
- [27] J.-H. Lee, T.-W. Lee, F. A. Jolesz, and S.-S. Yoo, "Independent vector analysis (IVA): Multivariate approach for fMRI group study," *NeuroImage*, vol. 40, no. 1, pp. 86–109, 2008.
- [28] T. Adalı, Y. Levin-Schwartz, and V. D. Calhoun, "Multi-modal data fusion using source separation: Two effective models based on ICA and IVA and their properties," *Proceedings of the IEEE*, vol. 103, no. 9, pp. 1478 – 1493, 2015.
- [29] A. M. Engberg, K. W. Andersen, M. Mørup, and K. H. Madsen, "Independent vector analysis for capturing common components in fMRI group analysis," in *Pattern Recognition in Neuroimaging (PRNI), 2016 International Workshop on*, 2016, pp. 1–4.
- [30] A. Michael, M. Anderson, R. Miller, T. Adalı, and V. D. Calhoun, "Preserving subject variability in group fMRI analysis: Performance evaluation of GICA versus IVA," *Frontiers in Systems Neuroscience*, vol. 8, pp. 106–123, 2014.
- [31] J. Laney, K. P. Westlake, S. Ma, E. Woytowicz, V. D. Calhoun, and T. Adalı, "Capturing subject variability in fMRI data: A graph-theoretical analysis of GICA vs. IVA," *Journal of Neuroscience Methods*, vol. 247, pp. 32–40, 2015.
- [32] M. Anderson, T. Adalı, and X.-L. Li, "Joint blind source separation with multivariate Gaussian model: Algorithms and performance analysis," *IEEE Transactions on Signal Processing*, vol. 60, no. 4, pp. 1672–1683, April 2012.
- [33] S. Bhinge, R. Mowakeaa, V. D. Calhoun, and T. Adalı, "Extraction of time-varying spatio-temporal networks using parameter-tuned constrained IVA," *IEEE Transactions on Medical Imaging*, 2019.
- [34] J. R. Kettenring, "Canonical analysis of several sets of variables," *Biometrika*, vol. 58, no. 3, pp. 433–451, 1971.
- [35] Y.-O. Li, T. Adalı, W. Wang, and V. D. Calhoun, "Joint blind source separation by multiset canonical correlation analysis," *IEEE Transactions on Signal Processing*, vol. 57, no. 10, pp. 3918–3929, 2009.
- [36] F. Deleus and M. M. Van Hulle, "Functional connectivity analysis of fMRI data based on regularized multiset canonical correlation analysis," *Journal of Neuroscience Methods*, vol. 197, pp. 143–157, 2011.
- [37] V. Kiviniemi, T. Starck, J. Remes, X. Long, J. Nikkinen, M. Haapea, J. Veijola, I. Moilanen, M. Isohanni, Y.-F. Zang *et al.*, "Functional segmentation of the brain cortex using high model order group PICA," *Human Brain Mapping*, vol. 30, no. 12, pp. 3865–3886, 2009.
- [38] E. A. Allen, E. B. Erhardt, E. Damaraju, W. Gruner, J. M. Segall, R. F. Silva, M. Havlicek, S. Rachakonda, J. Fries, R. Kalyanam *et al.*, "A baseline for the multivariate comparison of resting-state networks," *Frontiers in Systems Neuroscience*, vol. 5, p. 2, 2011.
- [39] S. R. Kay, A. Fiszbein, and L. A. Opler, "The positive and negative syndrome scale (PANSS) for schizophrenia," *Schizophrenia Bulletin*, vol. 13, no. 2, pp. 261–276, 1987.
- [40] A. Hyvärinen, J. Karhunen, and E. Oja, *Independent Component Analysis*. John Wiley & Sons, Inc., 2001.
- [41] T. Adalı, M. Anderson, and G.-S. Fu, "Diversity in independent component and vector analyses: Identifiability, algorithms, and applications in medical imaging," *IEEE Signal Processing Magazine*, vol. 31, no. 3, pp. 18–33, May 2014.
- [42] V. D. Calhoun, T. Adalı, G. D. Pearlson, and J. J. Pekar, "A method for making group inferences from functional MRI data using independent component analysis," *Human Brain Mapping*, vol. 14, no. 3, pp. 140–151, 2001.
- [43] K. Li, L. Guo, J. Nie, G. Li, and T. Liu, "Review of methods for functional brain connectivity detection using fMRI," *Computerized Medical Imaging and Graphics*, vol. 33, no. 2, pp. 131–139, 2009.
- [44] M. Anderson, G.-S. Fu, R. Phlypo, and T. Adalı, "Independent vector analysis: Identification conditions and performance bounds," *IEEE Transactions on Signal Processing*, vol. 62, no. 17, pp. 4399–4410, Sep. 2014.
- [45] M. Anderson, G.-S. Fu, R. Phlypo, and T. Adalı, "Independent vector analysis, the Kotz distribution, and performance bounds," in *2013 IEEE International Conference on Acoustics, Speech and Signal Processing (ICASSP)*, 2013, pp. 3243–3247.
- [46] Z. Boukouvalas, G.-S. Fu, and T. Adalı, "An efficient multivariate generalized gaussian distribution estimator: Application to IVA," in *2015 49th Annual Conference on Information Sciences and Systems (CISS)*, 2015, pp. 1–4.
- [47] V. D. Calhoun and T. Adalı, "Unmixing fMRI with independent component analysis," *IEEE Engineering in Medicine and Biology Magazine*, vol. 25, no. 2, pp. 79–90, 2006.
- [48] A. Scott, W. Courtney, D. Wood, R. De la Garza, S. Lane, R. Wang, M. King, J. Roberts, J. A. Turner, and V. D. Calhoun, "COINS: An innovative informatics and neuroimaging tool suite built for large heterogeneous datasets," *Frontiers in Neuroinformatics*, vol. 5, p. 33, 2011.
- [49] M. S. Çetin, F. Christensen, C. C. Abbott, J. M. Stephen, A. R. Mayer, J. M. Cañive, J. R. Bustillo, G. D. Pearlson, and V. D. Calhoun, "Thalamus and posterior temporal lobe show greater inter-network connectivity at rest and across sensory paradigms in schizophrenia," *NeuroImage*, vol. 97, pp. 117 – 126, 2014.
- [50] C. Aine, H. Bockholt, J. Bustillo, J. Cañive, A. Caprihan, C. Gasparovic, F. Hanlon, J. Houck, R. Jung, J. Lauriello *et al.*, "Multimodal neuroimaging in schizophrenia: Description and dissemination," *Neuroinformatics*, vol. 15, no. 4, pp. 343–364, 2017.
- [51] J. Shin, S. Ahn, and X. Hu, "Correction for the T1 effect incorporating flip angle estimated by Kalman filter in cardiac-gated functional MRI," *Magnetic Resonance in Medicine*, vol. 70, no. 6, pp. 1626–1633, 2013.
- [52] L. Freire, A. Roche, and J.-F. Mangin, "What is the best similarity measure for motion correction in fMRI time series?" *IEEE Transactions on Medical Imaging*, vol. 21, no. 5, pp. 470–484, 2002.
- [53] K. J. Friston, A. P. Holmes, K. J. Worsley, J. P. Poline, C. D. Frith, and R. S. J. Frackowiak, "Statistical parametric maps in functional imaging: A general linear approach," *Human Brain Mapping*, vol. 2, no. 4, pp. 189–210, 1994.
- [54] Y.-O. Li, T. Adalı, and V. D. Calhoun, "Estimating the number of independent components for functional magnetic resonance imaging data," *Human Brain Mapping*, vol. 28, no. 11, pp. 1251–1266, 2007.
- [55] X.-L. Li, S. Ma, V. D. Calhoun, and T. Adalı, "Order detection for fMRI analysis: Joint estimation of downsampling depth and order by information theoretic criteria," in *2011 IEEE International Symposium on Biomedical Imaging: From Nano to Macro*, April 2011, pp. 1019–1022.
- [56] G.-S. Fu, M. Anderson, and T. Adalı, "Likelihood estimators for dependent samples and their application to order detection," *IEEE Transactions on Signal Processing*, vol. 62, no. 16, pp. 4237–4244, Aug. 2014.
- [57] Q. Long, S. Bhinge, Y. Levin-Schwartz, Z. Boukouvalas, V. D. Calhoun, and T. Adalı, "The role of diversity in data-driven analysis of multi-subject fMRI data: Comparison of approaches based on independence and sparsity using global performance metrics," *Human Brain Mapping*, vol. 40, no. 2, pp. 489–504, 2019.
- [58] S.-i. Amari, "Estimating functions of independent component analysis for temporally correlated signals," *Neural Computation*, vol. 12, no. 9, pp. 2083–2107, Sep. 2000.
- [59] J. Sui, T. Adalı, G. D. Pearlson, and V. D. Calhoun, "An ICA-based method for the identification of optimal FMRI features and components using combined group-discriminative techniques," *NeuroImage*, vol. 46, no. 1, pp. 73–86, 2009.
- [60] K. Bhaganagarapu, G. D. Jackson, and D. F. Abbott, "An automated method for identifying artifact in independent component analysis of resting-state fMRI," *Frontiers in Human Neuroscience*, vol. 7, p. 343, 2013.
- [61] E. Bullmore, S. Frangou, and R. Murray, "The dysplastic net hypothesis: An integration of developmental and dysconnectivity theories of schizophrenia," *Schizophrenia Research*, vol. 28, no. 2, pp. 143–156, 1997.

- [62] K. E. Stephan, K. J. Friston, and C. D. Frith, "Dysconnection in schizophrenia: From abnormal synaptic plasticity to failures of self-monitoring," *Schizophrenia Bulletin*, vol. 35, no. 3, pp. 509–527, 2009.
- [63] K. J. Friston, "Schizophrenia and the disconnection hypothesis," *Acta Psychiatrica Scandinavica*, vol. 99, pp. 68–79, 1999.
- [64] M. E. Newman, "Modularity and community structure in networks," *Proceedings of the National Academy of Sciences*, vol. 103, no. 23, pp. 8577–8582, 2006.
- [65] A. Mucci, S. Galderisi, B. Kirkpatrick, P. Bucci, U. Volpe, E. Merlotti, F. Centanaro, F. Catapano, and M. Maj, "Double dissociation of N1 and P3 abnormalities in deficit and nondeficit schizophrenia," *Schizophrenia Research*, vol. 92, no. 1-3, pp. 252–261, 2007.
- [66] C. Arango, B. Kirkpatrick, and R. W. Buchanan, "Neurological signs and the heterogeneity of schizophrenia," *American Journal of Psychiatry*, vol. 157, no. 4, pp. 560–565, 2000.
- [67] N. Kanahara, Y. Sekine, T. Haraguchi, Y. Uchida, K. Hashimoto, E. Shimizu, and M. Iyo, "Orbitofrontal cortex abnormality and deficit schizophrenia," *Schizophrenia Research*, vol. 143, no. 2-3, pp. 246–252, 2013.
- [68] S. M. Silverstein, S. Berten, B. Essex, I. Kovacs, T. Susmaras, and D. M. Little, "An fMRI examination of visual integration in schizophrenia," *Journal of Integrative Neuroscience*, vol. 8, no. 02, pp. 175–202, 2009.
- [69] H. Takahashi, M. Koeda, K. Oda, T. Matsuda, E. Matsushima, M. Matsuura, K. Asai, and Y. Okubo, "An fMRI study of differential neural response to affective pictures in schizophrenia," *NeuroImage*, vol. 22, no. 3, pp. 1247–1254, 2004.
- [70] H. C. Whalley, V.-E. Gountouna, J. Hall, A. McIntosh, M.-C. Whyte, E. Simonotto, D. E. Job, D. G. Owens, E. C. Johnstone, and S. M. Lawrie, "Correlations between fMRI activation and individual psychotic symptoms in un-medicated subjects at high genetic risk of schizophrenia," *BMC Psychiatry*, vol. 7, no. 1, p. 61, 2007.
- [71] V. A. Vorobyev, K. Alho, S. V. Medvedev, S. V. Pakhomov, M. S. Roudas, J. M. Rutkovskaya, M. Tervaniemi, T. L. Van Zuijen, and R. Näätänen, "Linguistic processing in visual and modality-nonspecific brain areas: PET recordings during selective attention," *Cognitive Brain Research*, vol. 20, no. 2, pp. 309–322, 2004.
- [72] R. S. Patel, F. D. Bowman, and J. K. Rilling, "Determining hierarchical functional networks from auditory stimuli fMRI," *Human Brain Mapping*, vol. 27, no. 5, pp. 462–470, 2006.
- [73] X. Peng, S. Xiao, J. Feng, W.-Y. Yau, and Z. Yi, "Deep subspace clustering with sparsity prior," in *Proceedings of the Twenty-Fifth International Joint Conference on Artificial Intelligence*, 2016, pp. 1925–1931.
- [74] S. Bhinge, Q. Long, Y. Levin-Schwartz, Z. Boukouvalas, V. D. Calhoun, and T. Adalı, "Non-orthogonal constrained independent vector analysis: Application to data fusion," in *Acoustics, Speech and Signal Processing (ICASSP), 2017 IEEE International Conference on*, 2017, pp. 2666–2670.